ER Stress and Mitochondrial Perturbations Regulate Cell Death in Retinal Detachment: Exploring the Role of HIF1α

Bhavneet Kaur, Bruna Miglioranza Scavuzzi, Mengling Yang, Jingyu Yao, Lin Jia, Steven F. Abcouwer, and David N. Zacks

Kellogg Eye Center, Department of Ophthalmology and Visual Sciences, University of Michigan, Ann Arbor, Michigan, United States

Correspondence: David N. Zacks, Kellogg Eye Center, Department of Ophthalmology and Visual Sciences, University of Michigan, 1000 Wall St., Ann Arbor, MI 48105, USA; davzacks@umich.edu.

Received: March 14, 2024
Accepted: September 2, 2024
Published: September 26, 2024

Citation: Kaur B, Miglioranza Scavuzzi B, Yang M, et al. ER stress and mitochondrial perturbations regulate cell death in retinal detachment: Exploring the role of HIF1α. *Invest Ophthalmol Vis Sci.* 2024;65(11):39. https://doi.org/10.1167/iovs.65.11.39

Purpose. Retinal detachment (RD) leads to photoreceptor (PR) hypoxia due to separation from the retinal pigment epithelium (RPE). Hypoxia stabilizes retinal hypoxia-inducible factor 1-alpha (HIF1α), crucial for PR survival during RD. This study explores the regulatory role of HIF1α in PR cell survival pathways during RD.

Methods. Experimental RD was created in C57BL/6J and HIF1αΔrod mice by injecting 1% hyaluronic acid into the subretinal space. The 661W photoreceptor cells were exposed to hypoxic conditions. Markers of endoplasmic reticulum stress (ERS), mitophagy, and accumulation of polyubiquinated proteins were evaluated using RT-PCR and western blot analyses. Cell death of PR cells was quantified using trypan blue exclusion assay and TUNEL staining. Retinal cell death was assessed using a DNA fragmentation assay.

Results. In C57BL/6J mice and 661W cells, there were increases in HIF1α protein levels: 2.2-fold after RD ($P = 0.04$) and threefold after hypoxia ($P = 0.057$). Both the in vivo and in vitro RD models showed increased protein expression of ERS markers (including BIP, CHOP, and IRE1α), mitophagy markers (Parkin, PINK, and FUNDC1), and polyubiquitinated proteins. In 661W cells, hypoxia resulted in a loss of mitochondrial membrane potential, an increase in mitochondrial reactive oxygen species, and a decrease in intracellular adenosine triphosphate levels. Lack of HIF1α in rods blocked the upregulation of mitophagy markers after RD.

Conclusions. RD results in the activation of ERS, mitophagy, mitochondrial dysfunction, and accumulation of polyubiquitinated proteins. Results suggest a role for HIF1α in activation of the mitophagy pathway after RD, which may serve to protect the PR cells.

Keywords: retinal detachment, hypoxia-inducible factor 1-alpha, ER stress, mitochondrial dysfunction, mitophagy

Retinal detachment (RD) is a serious ocular condition characterized by the separation of the neurosensory retina from the underlying choroid and retinal pigment epithelium (RPE).[1,2] When RD occurs, the oxygen supply to photoreceptor (PR) cells is impaired, leading to hypoxia of these cells, induction of inflammation, and increase in reactive oxygen species (ROS) formation, all of which ultimately result in apoptotic PR death.[3,4] An interesting paradox exists regarding the timing of PR death after RD. The high metabolic demand of the PR cells would suggest that loss of oxygen and metabolic support from the choroid/RPE would result in early and massive PR loss. Clinical experience, however, shows that PR loss after RD is more gradual, and this provides a therapeutic window of opportunity for repairing the detachment and recovering some amount of vision. Work in experimental models has shown that, in addition to the rapid induction of cell death pathway activation, there is a concomitant and counteracting activation of pro-survival pathways such as autophagy.[5] We have previously shown that RD also results in the stabilization of hypoxia-inducible factor 1-alpha (HIF1α) and upregulation of various stress response genes.[6,7] Our previous work suggests that HIF1α stabilization is protective of PRs, yet the mechanism of this effect remains largely unknown.

HIF1α is a key transcription factor that plays a central role in the cellular response to hypoxia.[8,9] Under normoxic conditions, HIF1α is quickly hydroxylated and targeted for degradation.[10] Under hypoxic conditions such as those caused by RD, HIF1α is stabilized and translocates to the nucleus where it forms a heterodimer with HIF1β.[10] This complex binds to hypoxia response elements, leading to the transcriptional upregulation of various genes involved in angiogenesis, cell survival, and metabolism.[10,11]

The hypoxia of RD is associated with oxidative stress, inflammation, and generation of ROS resulting in activation of endoplasmic reticulum stress (ERS) and the unfolded protein response (UPR). Prolonged oxidative stress is often associated with mitochondrial dysfunction and can result in the triggering of apoptosis.[18,19]

Mitochondrial biogenesis is the process by which cells increase their mitochondrial mass and function to meet the cellular energy demands.[12] This process involves the replication of mitochondrial DNA and assembly of new mitochondria from pre-existing ones.[13] Mitochondrial biogenesis is regulated by several factors, including peroxisome proliferator-activated receptor gamma coactivator 1-alpha (PGC-1α) and nuclear respiratory factor 2 (NRF2).[14] On the other hand, mitophagy is a selective form of autophagy where damaged or dysfunctional mitochondria are selectively engulfed by autophagosomes for transport to and degradation by lysosomes.[15] In the retina, mitophagy plays a crucial role in maintaining cellular homeostasis and preventing the accumulation of damaged mitochondria.[16] During RD, the disruption of nutrient and oxygen supply and increased oxidative stress can lead to ocular mitochondrial dysfunction and cell death.[17] Mitophagy is triggered as a protective mechanism to eliminate these dysfunctional mitochondria and prevent further damage.[16]

In this study, we hypothesized that RD results in ERS, mitochondrial dysfunction, mitophagy, and increased accumulation of polyubiquinated proteins. We sought to understand the relationship between the activation of these pathways and HIF1α stabilization, and we tested these hypotheses using our in vivo rodent model of experimental RD, as well as our in vitro model of hypoxic PR cells.

Materials and Methods

Experimental Retinal Detachment

All animal experiments in this study adhered to the guidelines established by the Institutional Animal Care & Use Committee at the University of Michigan and followed the ARVO Statement for the Use of Animals in Ophthalmic and Visual Research. Male and female C57BL/6J mice were sourced from The Jackson Laboratory (Bar Harbor, ME, USA). The HIF1αΔrod mice were generated as previously described.[18] Mice were kept in a 12-hour light/dark cycle. For all experiments, mice were between 8 and 14 weeks of age. Detachments were created as previously described.[18–20] Briefly, mice were anesthetized using a combination of ketamine (16 mg/mL) and xylazine (2 mg/mL), adjusted according to their individual body weights. Pupils were dilated using phenylephrine 2.5% and tropicamide 1%. A small incision was made approximately 1 mm posterior to the limbus with a 31-gauge needle. Then, 1 to 2 µL of 1% sodium hyaluronate (Healon, #10240011; Johnson & Johnson Vision, Irvine, CA, USA) was carefully injected into the subretinal space to elevate the retina from the RPE. Animals were euthanized and eyes removed at either 24 hours (1 day) or 72 hours (3 days) following RD. Retina samples were harvested, snap-frozen in liquid nitrogen, and stored at –80°C until further use.

Cell Culture Model of Photoreceptor Hypoxia

For in vitro experiments, we used the 661W PR cell line, which was obtained from Muayyad Al-Ubaidi, PhD (University of Oklahoma Health Sciences Center, Oklahoma City, OK, USA).[21] Cells were cultured in Gibco Dulbecco's Modified Eagle Medium (DMEM, #11885084; Thermo Fisher Scientific, Waltham, MA, USA) supplemented with 10% fetal bovine serum (FBS, #35-015-CV; Corning, Corning, NY, USA), 1% Gibco penicillin–streptomycin (#15140122; Thermo Fisher Scientific), 32-mM putrescine, 40-µL/L β-mercaptoethanol, 40-µM hydrocortisone 21-hemisuccinate, and 40-µM progesterone. Cells were incubated at 37°C in a humidified atmosphere of 5% CO_2 and 95% air. Simulation of the hypoxia of detachment was performed as previously described[22] by placing the cultured 661W photoreceptor cell culture dishes in a specialized incubator chamber (Billups-Rothenberg, Del Mar, CA, USA) that was set at 37°C and filled with humidified hypoxic air (1% O_2, 5% CO_2, 94% N_2).

Pre-designed HIF1α small interfering RNA (siRNA, #4390771; Thermo Fisher Scientific) was used to silence HIF1α, and non-targeting siRNA (#4390843; Thermo Fisher Scientific) served as a negative control and was used at the same concentration. The 661W cells were seeded into six-well or 96-well plates. After 24 hours, each well was transfected with the appropriate siRNAs in Gibco Opti-MEM Reduced Serum Medium (#31985062; Thermo Fisher Scientific) with Invitrogen Lipofectamine RNAiMAX Transfection Reagent (#13778075; Thermo Fisher Scientific), following the supplier's protocol. The cells were incubated with the siRNAs for 12 hours. The medium was then replaced with complete growth medium, and the cells were incubated for an additional 24 hours. Subsequently, the cells were subjected to hypoxic conditions in the hypoxic chamber for 24 hours.[22]

Western Blot Analysis

Cells and retinal tissues were lysed using radioimmunoprecipitation assay (RIPA) buffer (#R0278; Sigma-Aldrich, St. Louis, MO, USA) containing Pierce phosphatase and protease inhibitors (#A32957 and #A32955, respectively; Thermo Fisher Scientific). Protein concentration was determined using the RC DC Protein Assay Kit (#5000120; Bio-Rad Laboratories, Hercules, CA, USA). Following this, 20 µg of protein was loaded into each well, separated using the 4–15% Mini-PROTEAN TGX Precast Protein Gels (#4561086; Bio-Rad Laboratories), and then transferred onto a polyvinylidene fluoride membrane (#1620177; Bio-Rad Laboratories). Subsequently, the membranes were blocked with 5% bovine serum albumin (BSA, #A7906; Sigma-Aldrich) in Tris-buffered saline (TBS, #1706435; Bio-Rad Laboratories), and incubated overnight at 4°C with the primary antibody. The following antibodies were used: anti-mouse CHOP (#2895, 1:1000; Cell Signaling Technology, Danvers, MA, USA); anti-rabbit pIRE1α (#NB100-2323SS, 1:1000; Novus Biologicals, Littleton, CO, USA); anti-mouse BiP/Grp78 (#610979, 1:1000; BD Biosciences, Franklin Lakes, NJ, USA); anti-mouse mono-and polyubiquitinylated conjugates (#BML-PW8810, 1:1000; Enzo Life Sciences, Long Island, NY, USA); anti-mouse caspase 3 (#NB100-56113, 1:1000; Novus Biologicals); anti-mouse HIF1α (#MAB1536, 1:1000; R&D Systems, Minneapolis, MN, USA), anti-rabbit FUNDC1 (#NBP1-81063, 1:1000; Novus Biologicals); anti-rabbit PINK1 (#NB100-493, 1:1000; Novus Biologicals); anti-rabbit Parkin (#NBP2-67017, 1:1000; Novus Biologicals); and anti-mouse PGC-1α (#sc-517380, 1:500; Santa Cruz Biotechnology, Dallas, TX, USA). Following three washes with a solution of 0.1% Tween 20 in TBS, membranes were incubated for 1 hour with the suitable secondary antibody: either anti-rabbit IgG, HRP linked (#7074S, 1:5000; Cell Signaling Technology), or anti-mouse IgG (#NA931, 1:8000; GE HealthCare, Chicago, IL, USA). For loading control, either anti-mouse Invitrogen GAPDH Monoclonal Antibody (#AM4300, 1:1000; Thermo Fisher Scientific) or Millipore-

Investigative Ophthalmology & Visual Science

Sigma anti-mouse α tubulin (#T6199, 1:1000; Sigma-Aldrich) antibodies were used. In this study, protein quantification was conducted utilizing single bands located within the appropriate molecular-weight region of each studied protein. However, for polyubiquitinated proteins, a different approach was employed. Given the heterogeneous nature of polyubiquitinated proteins, the wide range of mobilities of polyubiquitinated proteins extending across the gel from 50 kDa to 250 kDa in each lane was considered. Membranes were developed using the SuperSignal West Pico PLUS Chemiluminescent Substrate (#34580; Thermo Fisher Scientific). Finally, blots were imaged and analyzed using cSeries Capture Software (#c500; Azure Biosystems, Dublin, CA, USA).

Immunocytochemistry

For immunocytochemistry (ICC), cells were cultured on coverslips and then treated with a 4% paraformaldehyde solution for fixation. After fixation, the cells were permeabilized with 0.1% Triton X-100, blocked using 2% BSA, and subsequently subjected to an overnight incubation with the antibodies against FUNDC1 (1:250; Novus Biologicals) or anti-mouse LC3B (#83506, 1:250; Cell Signaling Technology). Following three washes, the cells were exposed to the appropriate secondary antibody, Goat anti-Rabbit IgG (H+L) Highly Cross-Adsorbed Secondary Antibody, Alexa Fluor 555 (#A-21429, 1:500; Thermo Fisher Scientific) or Goat anti-Mouse IgG (H+L) Highly Cross-Adsorbed Secondary Antibody, Alexa Fluor 488 (#A-11029, 1:500; Thermo Fisher Scientific) for 1 hour. Nuclear staining was with Invitrogen Hoechst (#H3570, 1:1000; Thermo Fisher Scientific) for 10 minutes. Finally, coverslips were affixed onto slides using a glycerol-based liquid mounting solution.

Images for ICC were acquired utilizing the Leica STELLARIS 8 FALCON Confocal Microscope with a 40× objective lens (Leica Microsystems, Wetzlar, Germany). To ensure specificity of the immunostaining, all experimental samples included negative controls, where the primary antibody was substituted with normal IgG (1 mg/mL).

RNA Extraction, cDNA Preparation, and Quantitative Reverse-Transcription PCR

Total RNA was extracted from retinal tissue using the RNeasy Plus Micro Kit (#74034; Qiagen Sciences, Hilden, Germany), following the manufacturer's instructions. The concentration and quality of RNA were assessed using a NanoDrop instrument (Thermo Fisher Scientific). Subsequently, complementary DNA (cDNA) was synthesized from the total RNA using the High-Capacity cDNA Reverse Transcription Kit (#4368813; Thermo Fisher Scientific), following the provided protocol. Quantitative reverse-transcription PCR (qRT-PCR) was conducted using a CFX384 Touch (Bio-Rad Laboratories), employing the following primer sequences:

Hspa5 (encoding GRP78/BiP)—forward, ACTTGGGGACCACCTATTCCT; reverse, ATCGCCAATCAGACGCTCC)[23]
Ddit3 (encoding CHOP)—forward, GGAGCTGGAAGCCTGGTATG; reverse, GGATGTGCGTGTGACCTCTG)[24]
Prkn (encoding Parkin)—forward, AAACCGGATGAGTGGTGAGT; reverse, AGCTACCGACGTGTCCTTGT)[25]
Tfam—forward, AGCCAGGTCCAGCTCACTAA; reverse, AAACCCAAGAAAGCATGTGG)[26]
Pgc1a (encoding PGC-1α)—forward, AGCCGTGACCACTGACAACGA; reverse, GCTGCATGGTTCTGAGTGCTA)[26]
Pink1—forward, GCTTGCCAATCCCTTCTATG; reverse, CTCTCGCTGGAGCAGTGAC)[27]
Pum1 (used as a housekeeping gene)—forward, ACAGCCTGCCAACACGTCCTTG; reverse, CCACTGCCAGTGTTGGAGTTTG[28]

Applied Biosystems Fast SYBR Green Master Mix (#4385612; Thermo Fisher Scientific) was also used. The total reaction volume was 10 µL. Relative gene expression levels were determined using the $\Delta\Delta C_T$ method.

Terminal Deoxynucleotidyl Transferase dUTP Nick-End Labeling

The 661W cells were grown on coverslips and exposed to hypoxia for different times, fixed using 4% paraformaldehyde, and processed for terminal deoxynucleotidyl transferase dUTP nick-end labeling (TUNEL) staining, using the DeadEnd Fluorometric TUNEL System (#G7360; Promega, Madison, WI, USA). Normoxic cells were used as the control group.

Trypan Blue Exclusion Assay

For the trypan blue exclusion assay, we initially placed cells at a density of 5×10^4 per well in 24-well flat-bottom culture plates. The next day, the cells were exposed to different durations of hypoxia in a hypoxia chamber. Following hypoxia exposure, we collected all cells, including those that had detached, and stained them with a 0.4% trypan blue solution for 2 minutes. Using a hemocytometer, we counted live cells (trypan blue–negative) and dead cells (trypan blue–positive). Then, we calculated the percentage of cell death by comparing it to the total number of cells.

DNA Fragmentation

DNA fragmentation was assessed using the Cell Death Detection ELISA kit (#11774425001; Roche, Basel, Switzerland). After harvesting, retinas were weighed and subsequently homogenized in lysis buffer using a plastic micropestle. Samples were then incubated for 30 minutes at room temperature under gentle shaking, followed by centrifugation (12,500 rpm for 10 minutes at 4°C). The supernatant was collected and transferred to the assay plate, and immunoreagents were added as per the manufacturer's instructions. Following a 2-hour incubation period and careful washing of the plate, Roche ABTS Solution was applied to each well, followed by incubation on a plate shaker (250 rpm) for 10 minutes. Finally, a stop solution was added, and the plate was read at 405 nm with a reference wavelength of 490 nm. Results were normalized by retinal mass.

Mitochondrial Functional Assays

Levels of intracellular adenosine triphosphate (ATP) were assessed using the ATPlite Luminescence Assay System kit (#6016941; PerkinElmer, Waltham, MA, USA) following the supplier's instructions. Briefly, 3×10^5 cells were seeded in six-well plates. After treatments, cell supernatant was collected, cells were washed twice with PBS, and lysis buffer was added to the wells and incubated for 5 minutes under

Investigative Ophthalmology & Visual Science

shaking. Then, 200 µL of PBS was added, and 150 µL of the resulting solution was transferred into a white microplate. Next, 50 µL of the substrate solution was added and luminescence evaluated. Quantitative analysis was performed after normalizing the results to untreated controls.

For evaluation of mitochondrial ROS and mitochondrial membrane potential, 1×10^4 cells were seeded in 96-well black/clear-bottom culture plates. For mitochondrial ROS, superoxide indicator Invitrogen MitoSOX (#M36008; Thermo Fisher Scientific) was used, following the supplier's instructions. Briefly, after the appropriate treatment period, cell growth media was aspirated, and cells underwent a 20-minute incubation at 37°C with 5-µM MitoSOX reagent in Gibco Hanks' Balanced Salt Solution (HBSS) media (#14025092; Thermo Fisher Scientific). Cells were gently washed three times with warm HBSS buffer, and fluorescence was measured using excitation/emission of 510/580 nm. Results were normalized to untreated controls.

Mitochondrial membrane potential ($\Delta\Psi_M$) was evaluated using Invitrogen Tetramethylrhodamine, Ethyl Ester, Perchlorate (TMRE) staining (#T669; Thermo Fisher Scientific) following the manufacturer's instructions. In short, after appropriate treatment time, the cell growth media were removed, and cells were incubated at 37°C for 20 minutes with a 250-nM TMRE reagent working solution in HBSS. Next, cells were washed twice with HBSS and fluorescence quantified with excitation/emission of 488/570 nm. Quantitative analysis was performed after normalizing the results to untreated controls.

Mitochondrial labeling with Invitrogen MitoTracker Red CMXRos Dye (#M46752; Thermo Fisher Scientific) was employed as an additional technique to assess mitochondrial membrane potential. Specifically, 3×10^5 cells were plated onto coverslips in six-well plates and subjected to appropriate treatments. Following treatment, cells were exposed to a 500-nM working solution of the MitoTracker probe in HBSS at 37°C for 20 minutes, as per the manufacturer's instructions. Subsequently, cells were washed with prewarmed HBSS and fixed with a 4% paraformaldehyde solution for 15 minutes at 37°C. Following fixation, cells were washed three times with PBS and imaged using a fluorescence microscope (excitation/emission of 579/599 nm). Results were normalized to untreated control.

The methylthiazolyldiphenyl–tetrazolium bromide (MTT) assay was employed to assess cellular viability and mitochondrial activity. Briefly, after an appropriate treatment period, the cells were washed once with PBS and incubated with a 0.5-mg/mL solution of Thiazolyl Blue Tetrazolium Bromide (#M5655; Sigma-Aldrich) for 3 hours. The crystals formed were then dissolved with isopropanol, and absorbance was measured at 540 nm.

To evaluate the role of ERS in mitochondrial function, the chemical chaperone 4-phenylbutyric acid (4-PBA, #SML0309; Sigma-Aldrich) and IRE1α inhibitor 8-formyl-7-hydroxy-4-methylcoumarin (4µ8C, #SML0949; Sigma-Aldrich) were utilized. In all cases, cells were incubated with the reagents for 2 hours before being subjected to hypoxia.

Statistical Analysis

Data are depicted as the mean ± standard error of the mean (SEM). Statistical analysis was conducted utilizing Prism 9.1.0 (GraphPad, Boston, MA, USA). Statistical analysis was performed using one-way ANOVA with repeated measures followed by Tukey's post hoc test or Šídák's multiple-comparisons test, unless otherwise specified. In graphs, asterisks (*) indicate statistical significance: $^*P < 0.05$, $^{**}P < 0.01$, $^{***}P < 0.001$, $^{****}P < 0.0001$.

Results

Hypoxia-Induced Initiation of Programmed Cell Death in 661W Cells

In RD, animal models and clinical studies have demonstrated that PR degeneration is primarily attributed to PR apoptosis.[29] To further elucidate the effect of RD-induced hypoxia on PR cells, we subjected 661W cells to hypoxia as previously described,[30] and cell death was assessed using the trypan blue exclusion assay, which is based on the principle of loss of membrane integrity upon cell death.[31] We detected a significant and progressive loss of cell viability, both in vivo in the RD mouse model, demonstrated by an increase in DNA fragmentation (Fig. 1A), as well as in vitro using 661W cells. In vitro, approximately 15% ($P < 0.0001$) and 37% ($P < 0.0001$) cell death were observed after 48 and 72 hours of hypoxia, respectively (Fig. 1B), whereas the normoxic control exhibited only 2% cell death. In 661W cells subjected to hypoxia, we further confirmed time-dependent increases in levels of pro-caspase-3, which has been reported to be a HIF-responsive gene,[32] as well as increases in levels of cleaved-caspase-3 (Fig. 1C). This correlated to a similar time-dependent increase in TUNEL-positive 661W cells subjected to hypoxia (Fig. 1D). These results correspond to our previously described findings in the mouse model of experimental detachment, suggesting that our in vitro hypoxia model approximates the in vivo pathology.

Retinal Detachment Triggers ERS and Protein Ubiquitination

ERS has been shown to have a causal role in retinal degeneration,[33–36] and several studies have suggested that ERS can be involved in the induction of apoptosis following RD.[37–40] To examine the levels of ERS in RD more comprehensively, we created RD in C57BL/6J mice and evaluated markers of the UPR at 1 and 3 days post retinal detachment (dprd). We observed a time-dependent increase in protein expression of the ERS markers BIP, CHOP, and p-IRE1α (Fig. 2A, Supplementary Fig. S1A). We also observed accumulation of polyubiquitinylated proteins (Fig. 2B). We further assessed mRNA expressions of *Hspa5* (encoding GRP78/BiP) and *Ddit3* (encoding CHOP/GADD153) in retinas and found high mRNA expression for both *Hspa5* and *Ddit3* at 1 dprd and 3 dprd (Figs. 2C, 2D). In addition, we evaluated the same markers in 661W cells subjected to 8 hours, 18 hours, and 24 hours of hypoxia, and we observed similar increases of protein markers of ERS, polyubiquitinated protein accumulation, and elevated mRNA expression of these markers (Figs. 2E–H, Supplementary Fig. S1B). Thus, our results further demonstrate similarities between the models.

Hypoxia Results in Mitochondrial Dysfunction

It is well established that there is significant crosstalk between the ER and mitochondria under various stress conditions.[41] To understand how RD affects mitochondrial function, we measured various mitochondrial function mark-

Investigative Ophthalmology & Visual Science

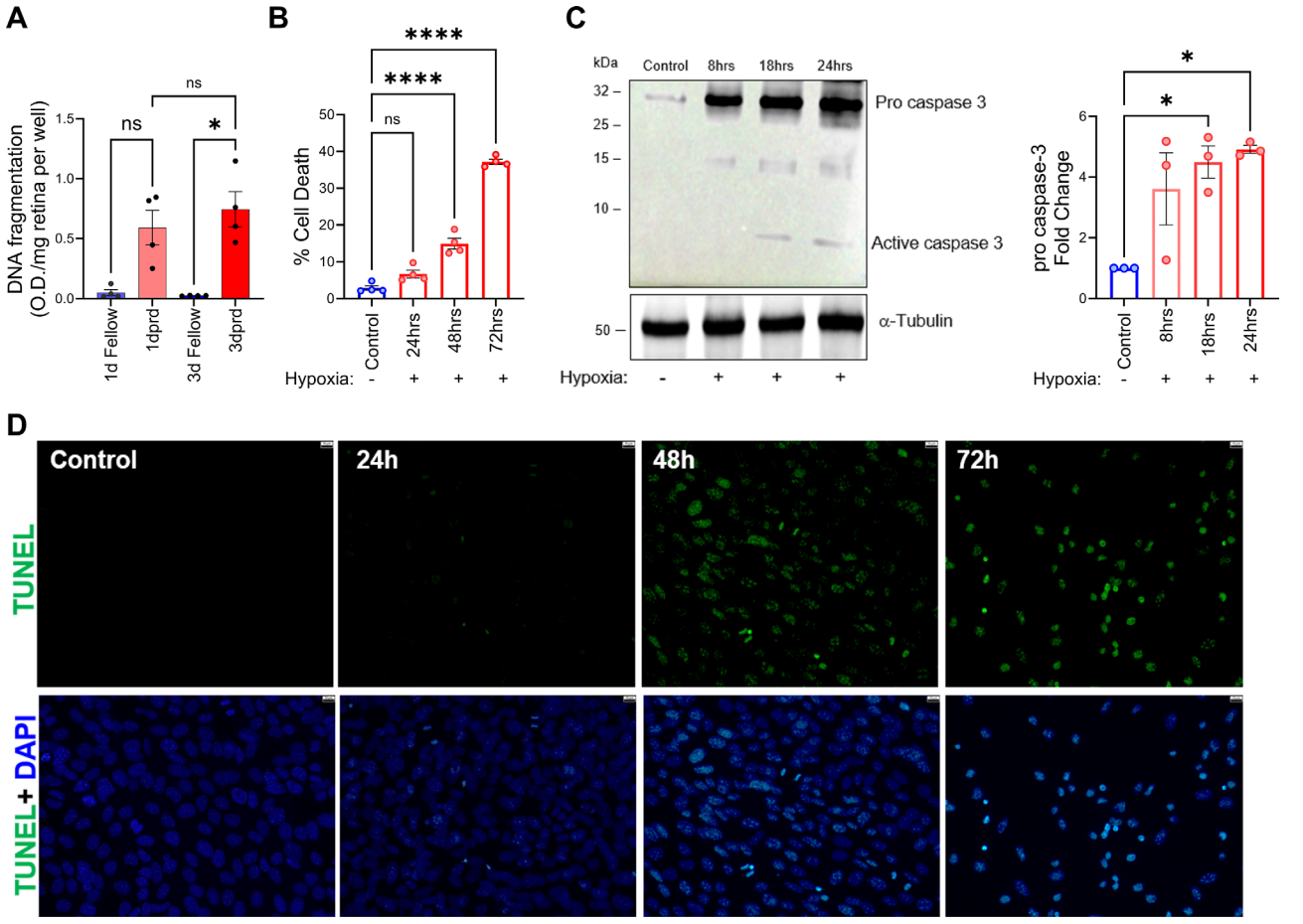

Figure 1. Hypoxia triggered time-dependent activation of programmed cell death in photoreceptor cells. (**A**) Cell death evaluation by DNA fragmentation assay in retinas of C57BL/6J mice at 1 day and 3 days following retinal detachment. (**B**) Cell death evaluation assessed by the trypan blue exclusion test in 661W cells subjected to 24 hours, 48 hours, and 72 hours of hypoxic conditions, compared to normoxic controls (21% oxygen). (**C**) Representative immunoblots of pro-caspase-3 and cleaved caspase-3 obtained from 661W cells subjected to 8 hours, 18 hours, and 24 hours of hypoxia (1% oxygen), compared to normoxic control (21% oxygen). Blots are representative of three independent experiments in each condition. (**D**) Qualitative detection of apoptotic cell death was assessed using the TUNEL assay. The 661W cells exhibited TUNEL staining after 48 and 72 hours of hypoxia. *Green* indicates TUNEL-positive cells; blue, DAPI. *Scale bar*: 10 µm. *Bar graphs* represent mean ± SEM. Statistical analysis was performed using one-way ANOVA with repeated measures followed by Tukey's post hoc test. *$P < 0.05$; ****$P < 0.0001$.

ers in PR cells under normoxic and hypoxic conditions. Mitochondrial function evaluation involves assessing metabolic activity and functional parameters, such as excessive production of mitochondrial ROS (mtROS) and changes in mitochondrial membrane potential.[42] In our study, we observed a decrease in mitochondrial membrane potential ($\Delta\Psi M$) in hypoxic 661W cells ($P < 0.0001$) compared to the normoxic controls (Figs. 3A, 3B), as measured using the mitotracker red and ratiometric fluorescence dye TMRE. Furthermore, when subjected to hypoxia, 661W cells displayed increased mitochondrial ROS ($P = 0.0149$) (Fig. 3C), reduced ATP levels ($P < 0.0001$) (Fig. 3D), and increased total ROS levels (Fig. 3E) as compared to the normoxic controls.

We hypothesized that crosstalk mechanisms between the ER and mitochondria lead to cell death. To test this, we employed a 2-hour pretreatment with the chemical chaperone 4-PBA, which inhibits ERS,[43] before subjecting 661W cells to hypoxia. We assessed mitochondrial membrane potential levels 24 hours after the onset of hypoxia exposure. Our findings confirmed that blocking ERS rescued hypoxia-induced mitochondrial abnormality in 661W cells (Fig. 3F). We also observed a reduction of total ROS levels with 4-PBA treatment (Fig. 3G). To confirm the role of ERS in the observed protective effects observed with 4-PBA, we used 4µ8C, an IRE1α inhibitor. This resulted in a 65% reduction in mitochondrial ROS generation under hypoxic conditions (Fig. 3H). These findings suggest that the ERS induced by hypoxia plays a causal role in mitochondrial impairment and in the generation of ROS.

We further investigated mitochondrial biogenesis, which is regulated by several factors, including PGC-1α, mitochondrial transcription factor A (TFAM), and NRF2.[14] In the mouse detachment model, we evaluated markers of mitochondrial biogenesis at 1 dprd and 3 dprd. We observed a decrease in the level of PGC1-α protein (Fig. 4A) and in the expression of *Pgc1a* and *Tfam* mRNAs in retinal samples obtained at 1 dprd and 3 dprd (Figs. 4B, 4C). This finding suggests that the disruption of these regulatory factors may contribute to the impairment of mitochondrial biogenesis in the context of RD.

Investigative Ophthalmology & Visual Science

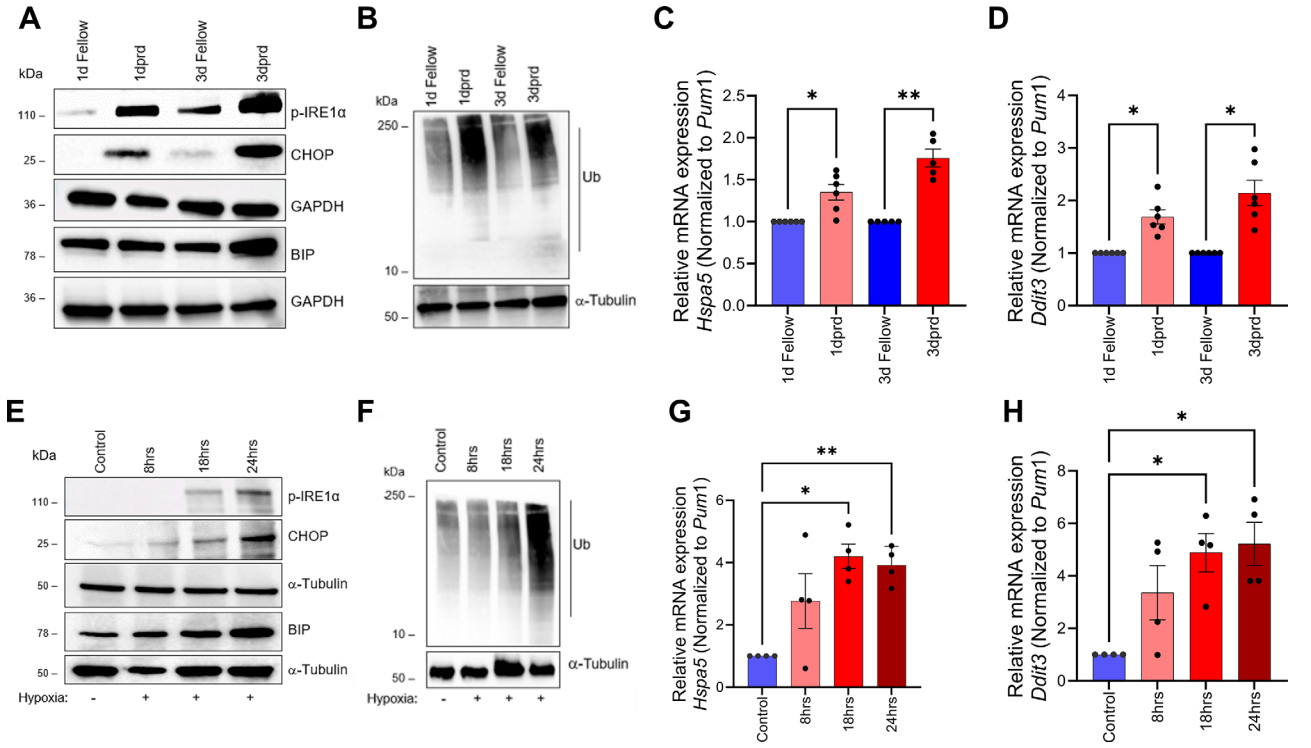

Figure 2. Retinal detachment and hypoxia triggered ERS and accumulation of protein polyubiquinated proteins. (**A**) Representative immunoblots of p-IRE1α, BIP, and CHOP proteins from retinas of C57BL/6J mice at 1 dprd and 3 dprd. Blots are representative of six independent animals in each condition; GAPDH was used as the loading control. (**B**) Representative immunoblots of polyubiquitinated proteins from retinas of C57BL/6J mice at 1 day and 3 days following retinal detachment. Blots are representative of three independent animals in each condition; α-tubulin was used as the loading control. (**C**) Relative mRNA expression of *Hspa5* obtained from retinas of C57BL/6J mice at 1 day ($n = 6$) and 3 days ($n = 5$) following retinal detachment. *Pum-1* was used as a housekeeping control gene for normalization. (**D**) Relative mRNA expression of *Ddit3* obtained from retinas of C57BL/6J mice at 1 day ($n = 6$) and 3 days ($n = 6$) following retinal detachment. *Pum-1* was used as a housekeeping control gene for normalization. (**E**) Representative immunoblots of p-IRE1α, BIP, and CHOP proteins from 661W cells subjected to 8 hours, 18 hours, and 24 hours of hypoxia. Blots are representative of three independent experiments in each condition; α-tubulin was used as loading control. (**F**) Representative immunoblots of polyubiquitinated proteins obtained from 661W cells subjected to 8 hours, 18 hours, and 24 hours of hypoxia. Blots are representative of three independent experiments in each condition; α-tubulin was used as loading control. (**G**) Relative mRNA expression of *Hspa5* (encoding GRP78) in 661W cells subjected to 8 hours, 18 hours, and 24 hours of hypoxia. *Pum-1* was used as a housekeeping control gene for normalization. (**H**) Relative mRNA expression of *Ddit3* (encoding CHOP) in 661W cells subjected to 8 hours, 18 hours, and 24 hours of hypoxia. *Pum-1* was used as a housekeeping control gene for normalization. *Bar graphs* represent mean ± SEM. Statistical analysis was performed using one-way ANOVA with repeated measures followed by Tukey's post hoc test. $^{*}P < 0.05$; $^{**}P < 0.01$.

Mitophagy Activated in Response to RD and Hypoxia

Mitophagy plays a critical role in maintaining cellular homeostasis in the retina and preventing the accumulation of damaged mitochondria.[26] When dysfunctional mitochondria are present, mitophagy is activated as a protective mechanism to eliminate these impaired organelles and prevent further damage.[26] To study the involvement of mitophagy in photoreceptors under the stress of RD, we examined mitophagy markers in 661W cells over varying durations of hypoxia. Additionally, we assessed mitophagy markers in mouse retinal samples collected at 1 dprd and 3 dprd. We found an increase in the protein expression of PTEN-induced kinase 1 (PINK1), Parkin, and FUN14 domain-containing 1 (FUNDC1) in 661W cells with increasing time of hypoxia (Fig. 5A, Supplementary Fig. S2A). We also observed the colocalization of FUNDC1 and LC3b in 661W cells under hypoxic conditions (Fig. 5B). This in vitro finding correlated with the upregulation of the mitophagy markers Parkin and FUNDC1 in retinal samples from detached mice (Fig. 5C, Supplementary Fig. S2B). We also evaluated gene expression levels of *Pink1* in mice samples (Fig. 5D), which were increased in both time points evaluated. However, *Prkn* (Fig. 5E) mRNA expression levels were not significantly different in RD samples as compared to the contralateral controls. These findings are consistent with the hypothesis that mitophagy is activated in response to hypoxia and RD.

HIF1α Is Associated With Mitophagy Induction After RD and Protection of Mitochondrial Function Following Hypoxia

Stabilization of HIF1α has been shown to trigger the activation of mitophagy.[44] Consistent with our previously published results,[18,30] we observed a trend for increases at 18 hours ($P = 0.0570$) and 24 hours ($P = 0.0825$) in HIF1α levels in hypoxic 661W cells (Fig. 6A, Supplementary Fig. S3A). We further observed that knocking down HIF1α resulted in a more detrimental effect on mitochondrial ROS levels (Supplementary Fig. S3C), as well as decreases in mitophagy

Investigative Ophthalmology & Visual Science

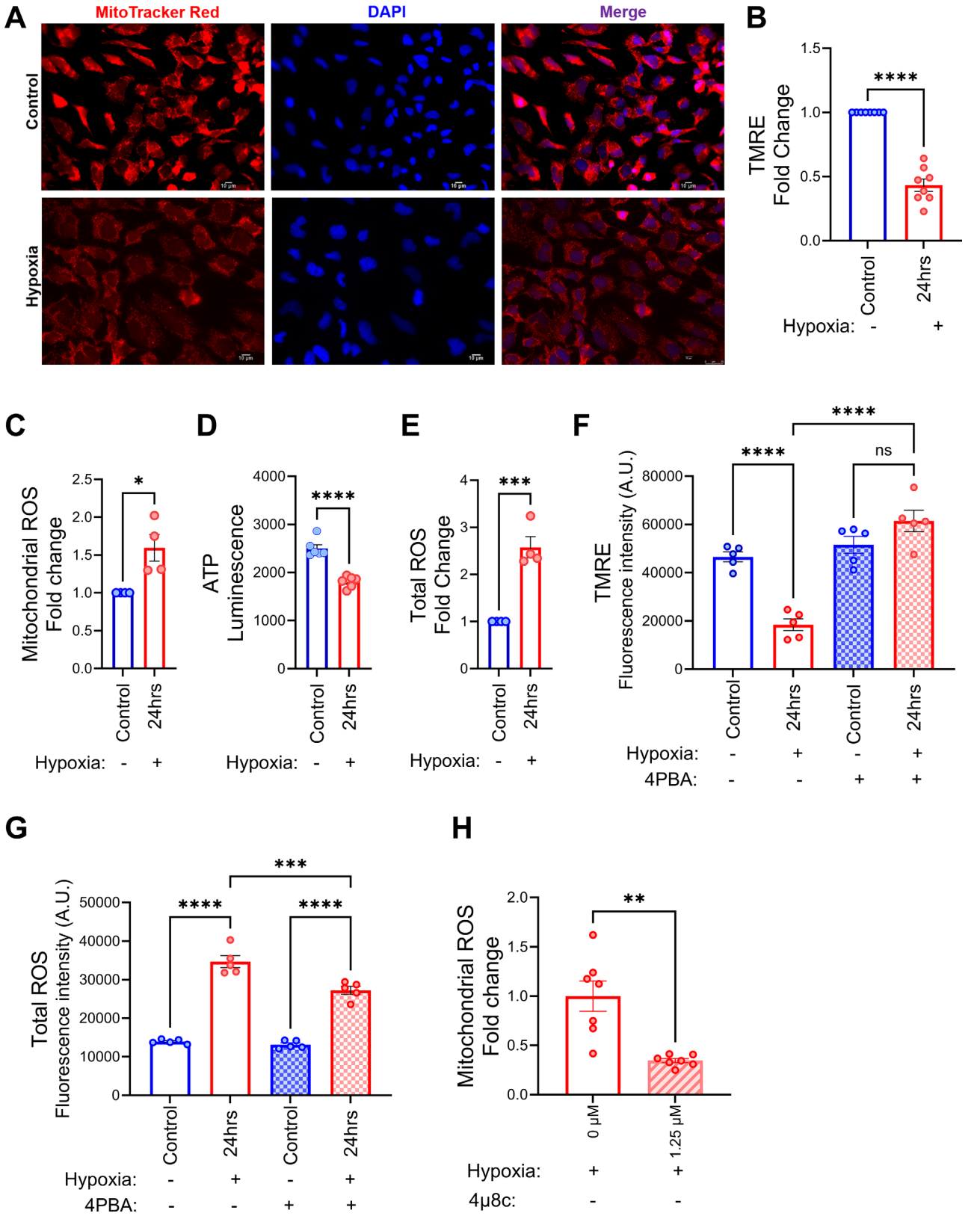

Figure 3. Retinal detachment in photoreceptors exposed to hypoxia leads to mitochondrial dysfunction and is reversed by chemical chaperone treatment. (**A**) Representative images of MitoTracker Red CMXRos–stained mitochondria (50 nM, 20 minutes) showing loss of mitochondrial membrane potential of 661W cells subjected to 24 hours of hypoxia compared to normoxic control. *Red* indicates MitoTracker-positive cells; blue, DAPI. *Scale bar*: 10 µm. (**B**) Mitochondrial membrane potential assessed by TMRE-stained (250 nM, 20 minutes) 661W cells subjected to 24 hours of hypoxia compared to normoxic control ($n = 8$). (**C**) Levels of mitochondrial ROS in 661W cells subjected to 24 hours of hypoxia compared to normoxic control, assessed with MitoSOX superoxide indicator ($n = 4$). (**D**) Intracellular ATP levels of 661W cells subjected to 24 hours of hypoxia compared to normoxic control ($n = 6$). Results are in relative light units (RLUs). (**E**) Levels of

Investigative Ophthalmology & Visual Science

total cellular ROS in 661W cells subjected to 24 hours of hypoxia compared to normoxic control, using dichlorodihydrofluorescein diacetate (DCFDA) probe. (**F**) Mitochondrial membrane potential assessed by TMRE probe in 661W cells subjected to 24 hours of hypoxia compared to normoxic control, in the presence (*unfilled bars*) or absence (*patterned bars*) of 5 mM of the chemical chaperone 4-PBA ($n = 5$). (**G**) Levels of total cellular ROS assessed by DCFDA probe in 661W cells subjected to 24 hours of hypoxia compared to normoxic control, in the presence (*unfilled bars*) or absence (*patterned bars*) of 5 mM of the chemical chaperone 4-PBA ($n = 5$). (**H**) Levels of mitochondrial ROS in 661W cells subjected to 24 hours of hypoxia, assessed with MitoSOX superoxide indicator in the presence (*unfilled bars*) or absence (*patterned bars*) of 1.25 µM of 4µ8C. *Bar graphs* represent mean ± SEM. Statistical analysis was performed using *t*-tests (**B**, **C**) or one-way ANOVA with repeated measures followed by Tukey's post hoc test (**F**, **G**). *$P < 0.05$; ***$P < 0.001$; ****$P < 0.0001$.

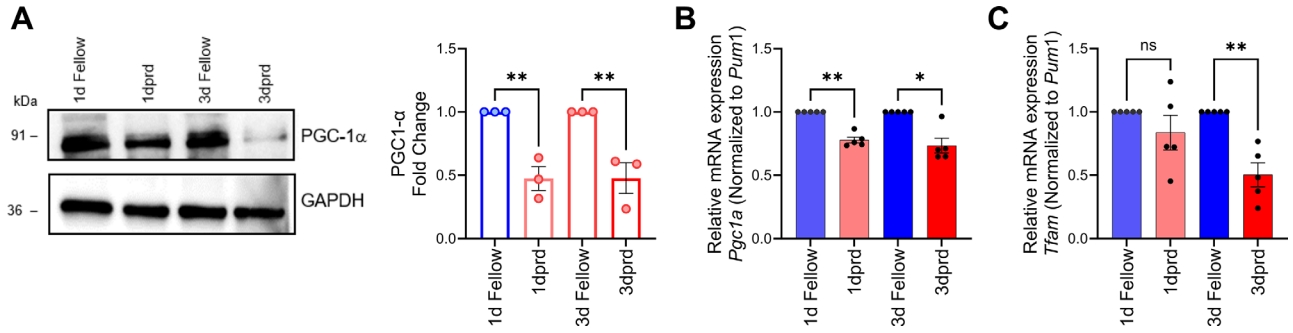

Figure 4. Retinal detachment in mice leads to mitochondrial perturbation. (**A**) Representative immunoblots and bar graph of PGC-1α proteins from retinas of C57BL/6J mice at 1 day and 3 days following retinal detachment. GAPDH was used as the loading control. (**B**) Relative mRNA expression of *Pgc1*a obtained at 1 dprd and 3 dprd compared to the contralateral eye (fellow). *Pum-1* was used as a housekeeping control gene for normalization. (**C**) Relative mRNA expression of *Tfam* obtained at 1 dprd and 3 dprd compared to the contralateral eye (fellow). *Pum-1* was used as a housekeeping control gene for normalization. *Bar graphs* represent mean ± SEM. Statistical analysis was performed using one-way ANOVA with repeated measures followed by Tukey's or Šídák's test. *$P < 0.05$; **$P < 0.01$.

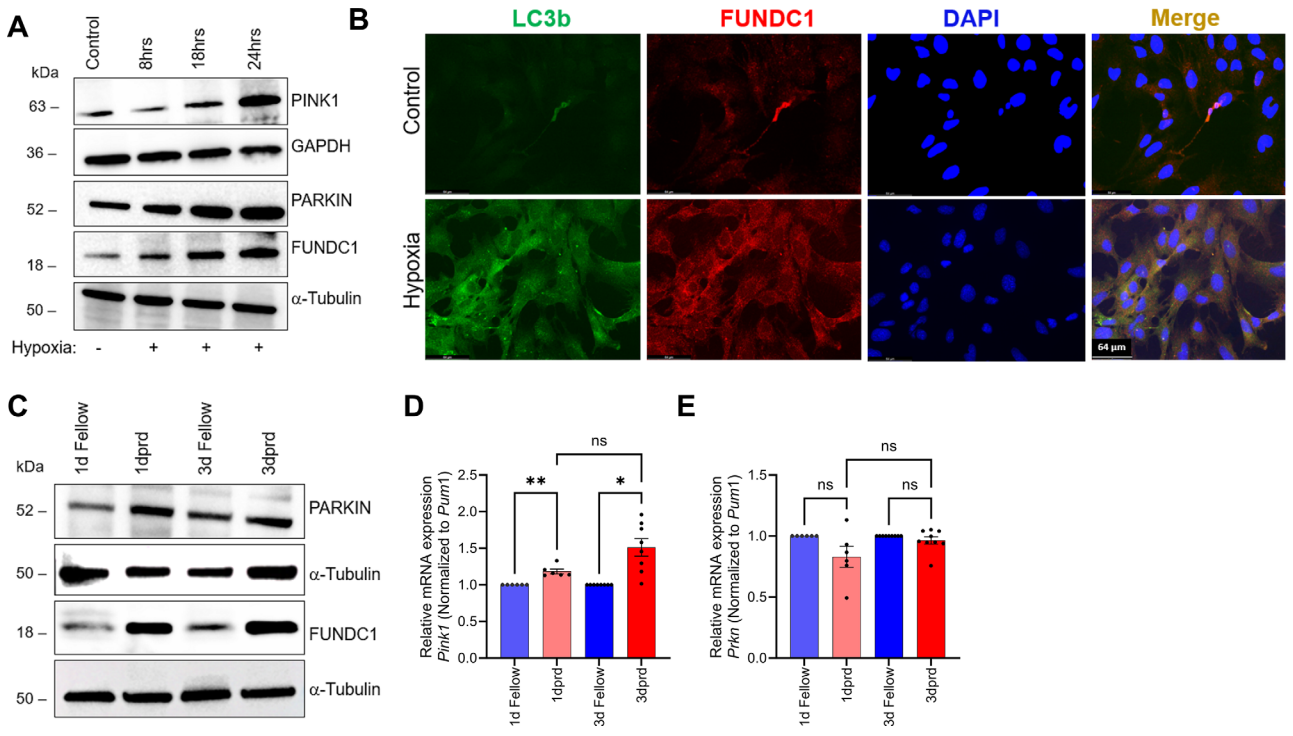

Figure 5. Hypoxia and retinal detachment activate mitophagy markers in retinal cells. (**A**) Representative immunoblots of PINK1, Parkin and FUNDC1 proteins from 661W cells subjected to 8 hours, 18 hours, and 24 hours of hypoxia. Blots are representative of three independent experiments in each condition; α-tubulin and GAPDH were used as loading controls. (**B**) Representative immunocytochemistry images of LC3B (*green*) and FUNDC1 (*red*) stained 661W cells subjected to 24 hours of hypoxia compared to normoxic control. *Scale bar*: 64 µm. (**C**) Representative immunoblots of Parkin and FUNDC1 proteins from retinas of C57BL/6J mice 1 day and 3 days following retinal detachment. Blots are representative of three independent animals in each condition; α-tubulin was used as the loading control. (**D**) Relative mRNA expression of *Pink1* obtained at 1 dprd and 3 dprd compared to the contralateral eye (fellow). *Pum-1* was used as a housekeeping control gene for normalization. (**E**) Relative mRNA expression of *Prkn* obtained at 1 dprd and 3 dprd compared to the contralateral eye (fellow). *Pum-1* was used as a housekeeping control gene for normalization. *Bar graphs* represent mean ± SEM. Statistical analysis was performed using one-way ANOVA with repeated measures followed by Tukey's test. *$P < 0.05$; **$P < 0.01$.

Investigative Ophthalmology & Visual Science

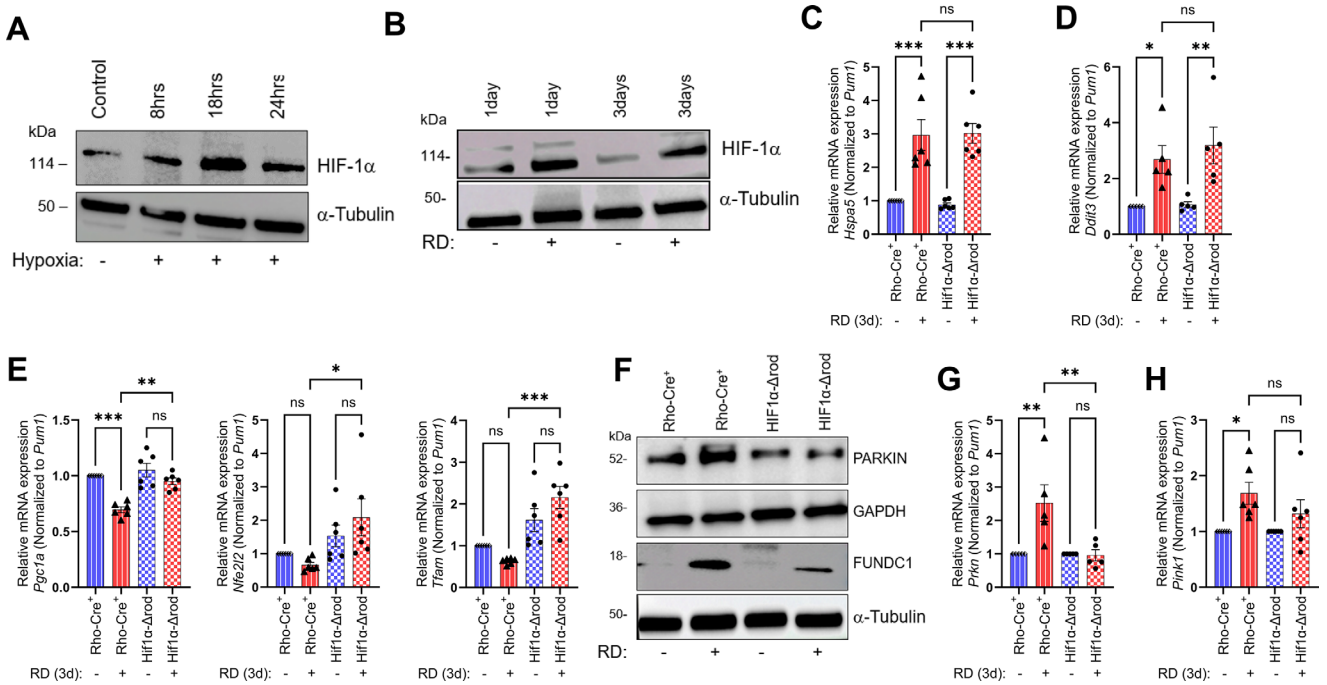

Figure 6. HIF1α is associated with mitophagy induction after RD in retinal cells. (**A**) Representative immunoblots of HIF1α protein from 661W cells subjected to 8 hours, 18 hours, and 24 hours of hypoxia. Blots are representative of three independent experiments in each condition; α-tubulin was used as the loading control. (**B**) Representative immunoblots of HIF1α protein from retinas of C57BL/6J mice at 1 dprd and 3 dprd. Blots are representative of three independent animals in each condition; α-tubulin was used as the loading control. (**C**) Relative mRNA expression of *Hspa5* obtained from retinas of Rho/Cre^{+} and HIF1αΔrod mice at 3 dprd compared to the contralateral eye (fellow). *Pum-1* was used as a housekeeping control gene for normalization. (**D**) Relative mRNA expression of *Ddit3* obtained from retinas of Rho/Cre^{+} and HIF1αΔrod mice at 3 dprd compared to the contralateral eye (fellow). *Pum-1* was used as a housekeeping control gene for normalization. (**E**) Relative mRNA expression of *Pgc1a* and *Tfam* obtained from retinas of Rho/Cre^{+} and HIF1αΔrod mice at 3 dprd compared to the contralateral eye (fellow). *Pum-1* was used as a housekeeping control gene for normalization. (**F**) Representative immunoblots of Parkin and FUNDC1 proteins from retinas of Rho/Cre^{+} and HIF1αΔrod mice at 3 dprd compared to the contralateral eye (fellow). GAPDH and α-tubulin were used as the loading control. (**G**) Relative mRNA expression of *Prkn* obtained from retinas of Rho/Cre+ and HIF1αΔrod mice at 3 dprd compared to the contralateral eye (fellow). *Pum-1* was used as a housekeeping control gene for normalization. (**H**) Relative mRNA expression of *Pink* obtained from retinas of Rho/Cre^{+} and HIF1αΔrod mice at 3 dprd compared to the contralateral eye (fellow). *Pum-1* was used as a housekeeping control gene for normalization. *Bar graphs* represent mean ± SEM. Statistical analysis was performed using two-way ANOVA with repeated measures followed by Tukey's test. *$P < 0.05$; **$P < 0.01$; ***$P < 0.001$.

markers such as Parkin, PINK1, and FUNDC1 (Supplementary Figs. S3D–S3F) in 661W cells. To strengthen our findings, we examined HIF1α expression in retinal samples from mice with RD. Consistent with the cellular system, the in vivo data also confirmed increased expression of HIF1α in RD samples (Fig. 6B, Supplementary Fig. S3G). We previously described the creation of a mouse strain with the conditional knockout of HIF1α in rod photoreceptors, which we denoted as the HIF1α rod.[18] To better understand the role of HIF stabilization in hypoxia-induced cellular pathways such as ERS, mitochondrial biogenesis, and mitophagy, we assessed the presence of their respective markers in the HIF1α rod mouse. We found that the ERS markers *Hspa5* and *Ddit3* did not exhibit any changes in HIF1α rod retinas at the mRNA level (Figs. 6C, 6D, Supplementary Fig. S3J). Additionally, mRNA expression of the mitochondrial biogenesis markers *Pgc1*a and *Tfam* were also not changed (Fig. 6E). However, we did find significant reductions in expression of the mitophagy markers *Pink1* and *Prkn* on the mRNA level, as well as FUNDC1 on the protein level. We observed that these markers, whose levels had previously increased in response to RD, exhibited a notable reduction in expression in HIF1α rod retinas (Figs. 6F–H, Supplementary Figs. S3H, S3I). These findings suggest that HIF1α has a role as a regulator of mitophagy within the context of RD. The summary of key findings of this study are illustrated in Supplementary Figure S4.

Discussion

In RD, the neurosensory retina is separated from the underlying RPE, leading to hypoxia and the stabilization of HIF1α. In addition, there is a significant disruption of retinal functional and nutritional balances, eventually leading to PR degeneration.[2] We and others have previously demonstrated that the primary mechanism driving PR death following detachment is apoptotic.[45,46] We have also shown that HIF is stabilized after RD and results in the transcriptional activation of HIF response genes.[18] Here, we aimed to investigate the impact of HIF1α stabilization on downstream regulators of cell death and cell survival—in particular, the effect of HIF on the ERS/UPR response and mitophagy. Using both in vitro and in vivo models of RD, we demonstrated that HIF is less involved in the former and more in the latter.

Previous studies have suggested that HIF1α levels can be regulated by ERS.[47] It has also been demonstrated that ERS markers are elevated and can correlate with the apoptosis of retinal cells after RD, as well as induce inflammation and the

Investigative Ophthalmology & Visual Science

generation of ROS.[37–40] In our study, we observed increases in markers of ERS, which gradually increased over time (specifically, GRP78, CHOP, and p-IRE1α). The ERS marker elevation was inversely associated with the loss of cell viability, which suggested that ERS may have a central role in the promotion of cell death in RD. Ubiquitination helps mark short-lived proteins for destruction in eukaryotic cells. In our study, we found that, after 661W cells were exposed to hypoxia and in mice samples after RD, there was a time-dependent increase in polyubiquinilated proteins. Under homeostatic conditions, the proteasome efficiently breaks down these tagged proteins. However, when there is an accumulation of misfolded or aggregated proteins, or certain mutant proteins, it can overwhelm the proteasome. This leads to a general decrease in the ability of the proteasome to function and may trigger the UPR.[48–50] The mechanisms behind this are not fully understood but may involve disruptions with proteasome components connected to the ER or the AAA+ ATPase Cdc48, affecting ER-associated degradation. Future studies will explore how ERS and HIF1α impact proteasomal degradation following RD and whether these pathways are interconnected or independent.

Due to the well-established crosstalk between the ERS and mitochondria,[41] we sought to assess mitochondrial function and whether or not it is impacted by RD. In our study, we observed the presence of mitochondrial abnormalities marked by loss of mitochondrial membrane potential, increase of mitochondrial ROS levels, and decrease in mitochondrial biogenesis markers, including PGC1-α, NRF2, and TFAM, following RD. However, it is noteworthy that these abnormalities were only evident at later time points and not during the early stages, suggesting that mitochondrial abnormalities represent a progressive dysfunction due to prolonged stress in RD and/or these are secondary to upstream activation of other pathways. Our research further suggests that ERS serves as a contributor to mitochondrial dysfunction following RD. Blocking ERS with the chaperone 4-PBA successfully prevented the loss of mitochondrial membrane potential. However, although 4-PBA treatment was able to significantly reduce ROS generation, the reduction was not complete, indicating that there may be additional contributors of ROS in response to hypoxia, or that the 4-PBA is not completely (100%) effective.[51] To further investigate, we tested an additional ERS inhibitor, 4μ8C, which also resulted in a significant, yet incomplete reduction in mitochondrial ROS generation.

Mitochondria, the primary organelle for energy production, also plays a central role in maintaining intracellular homeostasis. The preservation of mitochondrial function and integrity is paramount for sustaining normal cell physiology.[52,53] The removal of impaired mitochondria through mitophagy is essential in preventing elevated levels of ROS, which play a significant role in the death of photoreceptors following RD. The elimination of damaged mitochondria has been demonstrated to be associated with a neuroprotective effect on photoreceptors after RD.[4,54,55] Our present findings reveal an increase in mitophagy markers such as Parkin, PINK1, and FUNDC1 following RD. This suggests the involvement of mitophagy in the context of RD. In our earlier research, our group has demonstrated the activation of pro-survival pathways, particularly the interleukin-6 pathway and the autophagy pathway, in response to RD.[21,56]

Our lab has shown that the initiation of survival pathways, including autophagy, depends on the presence of HIF1α during the early stages of RD.[22] In previous work, we have also demonstrated that RD can increase the expression of BCL2/adenovirus e1B 19-kDa protein interacting protein 3 (BNIP3),[30] a protein that plays a key role in the mediation of mitophagy, particularly under hypoxic conditions.[57] Additionally, it has been shown that HIF1 stabilization with prolyl-4-hydroxylases inhibitor increases the expression of BNIP3 and FUNDC1, key markers of mitophagy.[58] In the present study, we utilized rod HIF1α knockout mice and HIF1α knockdown 661W cells and demonstrated that the levels of mitophagy markers decrease when HIF1α is absent. We also found that knocking down HIF1α results in increased levels of mitochondrial ROS. Our data indicate that HIF1α stabilization acts to regulate pro-survival pathways, preserving mitochondrial function and mitigating apoptotic cell death, indicating a central role of HIF1α stabilization in the promotion of photoreceptor survival following RD.

Interestingly, the ERS pathway did not exhibit any significant changes in the HIF1α KO mice samples, suggesting that it is activated independently of HIF1α. Furthermore, we observed that mitochondrial biogenesis markers, particularly PGC1-α, were not reduced at the mRNA level in the HIF1αΔrod mice, contrary to what is observed in B6 and of Rho/Cre^{+} mice.

In summary, we have begun to demonstrate the intricate interplay among hypoxia, ERS, mitochondrial dysfunction, and apoptosis in the context of RD. We have identified a sequential chain of events, starting with hypoxia-induced ERS, which subsequently triggers mitochondrial dysfunction. Notably, we emphasize the pivotal role of HIF1α as a key player in the survival pathway, particularly in mitophagy, following RD. This finding underscores the potential of targeting ERS and promoting mitophagy to devise innovative treatment strategies for improving PR survival after RD. Future research will focus on further examining and defining the mechanisms governing the activation of mitophagy and ERS pathways by hypoxia and HIF1α.

Acknowledgments

Disclosure: **B. Kaur**, None; **B. Miglioranza Scavuzzi**, None; **M. Yang**, None; **J. Yao**, None; **L. Jia**, None; **S.F. Abcouwer**, None; **D.N. Zacks**, None

References

1. Blair K, Czyz C. *Retinal Detachment*. Treasure Island, FL: StatPearls Publishing; 2022.
2. Ghazi N, Green W. Pathology and pathogenesis of retinal detachment. *Eye (Lond)*. 2002;16:411–421.
3. Murakami Y, Notomi S, Hisatomi T, et al. Photoreceptor cell death and rescue in retinal detachment and degenerations. *Prog Retin Eye Res*. 2013;37:114–140.
4. Roh M, Murakami Y, Thanos A, Vavvas D, Miller J.Edaravone, an ROS scavenger, ameliorates photoreceptor cell death after experimental retinal detachment. *Invest Ophthalmol Vis Sci*. 2011;52:3825–3831.
5. Xiao J, Yao J, Jia L, et al. Autophagy activation and photoreceptor survival in retinal detachment. *Exp Eye Res*. 2021;205:108492.
6. Linsenmeier R, Padnick-Silver L. Metabolic dependence of photoreceptors on the choroid in the normal and detached retina. *Invest Ophthalmol Vis Sci*. 2000;41:3117–3123.
7. Wang S, Linsenmeier R. Hyperoxia improves oxygen consumption in the detached feline retina. *Invest Ophthalmol Vis Sci*. 2007;48:1335–1341.

8. Semenza G. Hypoxia-inducible factors in physiology and medicine. *Cell*. 2012;148:399–408.
9. Rocha S. Gene regulation under low oxygen: holding your breath for transcription. *Trends Biochem Sci*. 2007;32:389–397.
10. Vadlapatla R, Vadlapudi A, Mitra A. Hypoxia-inducible factor-1 (HIF-1): a potential target for intervention in ocular neovascular diseases. *Curr Drug Targets*. 2013;14:919–935.
11. Kaluz S, Kaluzová M, Stanbridge E. Regulation of gene expression by hypoxia: integration of the HIF-transduced hypoxic signal at the hypoxia-responsive element. *Clin Chim Acta*. 2008;395:6–13.
12. Popov L. Mitochondrial biogenesis: an update. *J Cell Mol Med*. 2020;24:4892–4899.
13. Ploumi C, Daskalaki I, Tavernarakis N. Mitochondrial biogenesis and clearance: a balancing act. *FEBS J*. 2017;284:183–195.
14. Hees J, Harbauer A. Metabolic regulation of mitochondrial protein biogenesis from a neuronal perspective. *Biomolecules*. 2022;12:1595.
15. Ding W, Yin X. Mitophagy: mechanisms, pathophysiological roles, and analysis. *Biol Chem*. 2012;393:547–564.
16. Jiménez-Loygorri J, Benítez-Fernández R, Viedma-Poyatos Á, et al. Mitophagy in the retina: viewing mitochondrial homeostasis through a new lens. *Prog Retin Eye Res*. 2023;96:101205.
17. Moos W, Faller D, Glavas I, et al. Treatment and prevention of pathological mitochondrial dysfunction in retinal degeneration and in photoreceptor injury. *Biochem Pharmacol*. 2022;203:115168.
18. Ross B, Jia L, Kong D, et al. Hypoxia-inducible factor-1α in rods is neuroprotective following retinal detachment. *Invest Ophthalmol Vis Sci*. 2022;63:7.
19. Zacks D, Hänninen V, Pantcheva M, Ezra E, Grosskreutz C, Miller J. Caspase activation in an experimental model of retinal detachment. *Invest Ophthalmol Vis Sci*. 2003;44:1262–1267.
20. Kiang L, Ross B, Yao J, et al. Vitreous cytokine expression and a murine model suggest a key role of microglia in the inflammatory response to retinal detachment. *Invest Ophthalmol Vis Sci*. 2018;59:3767–3778.
21. Chinskey N, Zheng Q, Zacks D. Control of photoreceptor autophagy after retinal detachment: the switch from survival to death. *Invest Ophthalmol Vis Sci*. 2014;55:688–695.
22. Kaur B, Scavuzzi BM, Abcouwer SF, Zacks DN. A simplified protocol to induce hypoxia in a standard incubator: a focus on retinal cells. *Exp Eye Res*. 2023;236:109653.
23. Treacy-Abarca S, Mukherjee S. *Legionella* suppresses the host unfolded protein response via multiple mechanisms. *Nat Commun*. 2015;6:1–10.
24. Cao Y, Trillo-Tinoco J, Sierra R, et al. ER stress-induced mediator C/EBP homologous protein thwarts effector T cell activity in tumors through T-bet repression. *Nat Commun*. 2019;10:1280.
25. Bouman L, Schlierf A, Lutz A, et al. Parkin is transcriptionally regulated by ATF4: evidence for an interconnection between mitochondrial stress and ER stress. *Cell Death Differ*. 2011;18:769–782.
26. Guo X, Dason E, Zanon-Moreno V, et al. PGC-1α signaling coordinates susceptibility to metabolic and oxidative injury in the inner retina. *Am J Pathol*. 2014;184:1017–1029.
27. Choi I, Choi D, Yang H, et al. PINK1 expression increases during brain development and stem cell differentiation, and affects the development of GFAP-positive astrocytes. *Mol Brain*. 2016;9:5.
28. de Jonge H, Fehrmann R, de Bont E, et al. Evidence based selection of housekeeping genes. *PLoS One*. 2007;2:e898.
29. Besirli C, Chinskey N, Zheng Q, Zacks D. Inhibition of retinal detachment-induced apoptosis in photoreceptors by a small peptide inhibitor of the Fas receptor. *Invest Ophthalmol Vis Sci*. 2010;51:2177–2184.
30. Shelby S, Angadi P, Zheng Q, Yao J, Jia L, Zacks D. Hypoxia inducible factor 1α contributes to regulation of autophagy in retinal detachment. *Exp Eye Res*. 2015;137:84–93.
31. Strober W. Trypan blue exclusion test of cell viability. *Curr Protoc Immunol*. 2015;111:A3.B.1–A3.B.3.
32. Van Hoecke M, Prigent-Tessier A, Garnier P, et al. Evidence of HIF-1 functional binding activity to caspase-3 promoter after photothrombotic cerebral ischemia. *Mol Cell Neurosci*. 2007;34:40–47.
33. Roybal C, Marmorstein L, Vander Jagt D, Abcouwer S. Aberrant accumulation of fibulin-3 in the endoplasmic reticulum leads to activation of the unfolded protein response and VEGF expression. *Invest Ophthalmol Vis Sci*. 2005;46:3973–3979.
34. Ryoo H, Domingos P, Kang M, Steller H. Unfolded protein response in a *Drosophila* model for retinal degeneration. *EMBO J*. 2007;26:242–252.
35. Shimazawa M, Ito Y, Inokuchi Y, Hara H. Involvement of double-stranded RNA-dependent protein kinase in ER stress-induced retinal neuron damage. *Invest Ophthalmol Vis Sci*. 2007;48:3729–3736.
36. Sarkar H, Toms M, Moosajee M. Involvement of oxidative and endoplasmic reticulum stress in *RDH12*-related retinopathies. *Int J Mol Sci*. 2021;22:8863.
37. Liu H, Qian J, Wang F, et al. Endoplasmic reticulum stress participates in the cell apoptosis process in experimental retinal detachment. *Zhonghua Yan Ke Za Zhi*. 2008;44:800–806.
38. Liu H, Qian J, Wang F, et al. Expression of two endoplasmic reticulum stress markers, *GRP78* and *GADD153*, in rat retinal detachment model and its implication. *Eye (Lond)*. 2010;24:137–144.
39. Zhu H, Qian J, Wang W, et al. RNA interference of *GADD153* protects photoreceptors from endoplasmic reticulum stress-mediated apoptosis after retinal detachment. *PLoS One*. 2013;8:e59339.
40. Yan Q, Zhu H, Wang F, et al. Inhibition of TRB3 protects photoreceptors against endoplasmic reticulum stress-induced apoptosis after experimental retinal detachment. *Curr Eye Res*. 2016;41:240–248.
41. Cao S, Kaufman R. Endoplasmic reticulum stress and oxidative stress in cell fate decision and human disease. *Antioxid Redox Signal*. 2014;21:396–413.
42. Brand M, Nicholls D. Assessing mitochondrial dysfunction in cells. *Biochem J*. 2011;435:297–312.
43. Koyama M, Furuhashi M, Ishimura S, et al. Reduction of endoplasmic reticulum stress by 4-phenylbutyric acid prevents the development of hypoxia-induced pulmonary arterial hypertension *Am J Physiol Heart Circ Physiol*. 2014;306:H1314–H1323.
44. Hu S, Zhang C, Ni L, et al. Stabilization of HIF-1α alleviates osteoarthritis via enhancing mitophagy. *Cell Death Dis*. 2020;11:481.
45. Zacks D, Boehlke C, Richards A, Zheng Q. Role of the Fas-signaling pathway in photoreceptor neuroprotection. *Arch Ophthalmol*. 2007;125:1389–1395.
46. Zacks D, Zheng Q, Han Y, Bakhru R, Miller J. FAS-mediated apoptosis and its relation to intrinsic pathway activation in an experimental model of retinal detachment. *Invest Ophthalmol Vis Sci*. 2004;45:4563–4569.
47. López-Hernández B, Ceña V, Posadas I. The endoplasmic reticulum stress and the HIF-1 signalling pathways are involved in the neuronal damage caused

Investigative Ophthalmology & Visual Science

by chemical hypoxia. *Br J Pharmacol*. 2015;172:2838–2851.
48. Dantuma N, Lindsten K. Stressing the ubiquitin–proteasome system. *Cardiovasc Res*. 2010;85:263–271.
49. Mann D, Frankel A. Endocytosis and targeting of exogenous HIV-1 Tat protein. *EMBO J*. 1991;10:1733–1739.
50. Korolchuk V, Menzies F, Rubinsztein D. Mechanisms of cross-talk between the ubiquitin-proteasome and autophagy-lysosome systems. *FEBS Lett*. 2010;584:1393–1398.
51. Okoye C, Koren S, Wojtovich A. Mitochondrial complex I ROS production and redox signaling in hypoxia. *Redox Biol*. 2023;67:102926.
52. Li A, Gao M, Jiang W, Qin Y, Gong G. Mitochondrial dynamics in adult cardiomyocytes and heart diseases. *Front Cell Dev Biol*. 2020;8:584800.
53. Gong G, Song M, Csordas G, Kelly D, Matkovich S, Dorn GN. Parkin-mediated mitophagy directs perinatal cardiac metabolic maturation in mice. *Science*. 2015;350:aad2459.
54. Mazure N, Pouysségur J. Hypoxia-induced autophagy: cell death or cell survival? *Curr Opin Cell Biol*. 2010;22:177–180.
55. Mantopoulos D, Murakami Y, Comander J, et al. Tauroursodeoxycholic acid (TUDCA) protects photoreceptors from cell death after experimental retinal detachment. *PLoS One*. 2011;6:e24245.
56. Besirli C, Chinskey N, Zheng Q, Zacks D. Autophagy activation in the injured photoreceptor inhibits Fas-mediated apoptosis. *Invest Ophthalmol Vis Sci*. 2011;52:4193–4199.
57. He Y, Li J, Gong S, et al. BNIP3 phosphorylation by JNK1/2 promotes mitophagy via enhancing its stability under hypoxia. *Cell Death Dis*. 2022;13:966.
58. Liu H, Zhu H, Li T, Zhang P, Wang N, Sun X. Prolyl-4-hydroxylases inhibitor stabilizes HIF-1α and increases mitophagy to reduce cell death after experimental retinal detachment. *Invest Ophthalmol Vis Sci*. 2016;57:1807–1815.

Investigative Ophthalmology & Visual Science